

A Circularly Polarized Antenna for Dual Band Operation at 2.45 GHz and 5.10 GHz

Stefano Maddio^{*}, Giuseppe Pelosi, Monica Righini, and Stefano Selleri

Abstract—This paper describes the design and experimental characterization of a circular polarized printed antenna for dual-band WiFi operation at 2.45 GHz and 5.10 GHz. The patch design is based on a combination of slits loading and gap-coupling applied to a disc patch in order to enhance the radiation performances in terms of polarization purity and bandwidth at the two operation frequencies. Experimental validations confirm a maximum gain around 6.0 dB for both 2.45 and 5.10 GHz, as well as an axial ratio as low as 0.5 dB and a return loss exceeding 15 dB on the operating frequencies. These characteristics are suitable for operation in IEEE802.11x networks.

1. INTRODUCTION

Printed antennas operating in circular polarization (CP) are advantageous in modern communication applications because of their inherent robustness in both indoor and outdoor scenarios [1–4] and the capability to establish reliable links regardless of their relative orientation. In the field of indoor positioning, antennas with moderate to high directivity are also recommended [5, 6]. Furthermore, CP is an additional useful feature to improve the positioning accuracy [7]. Dual-Band CP operation is often a useful feature, as for the case of satellite communication [8].

Recently, the developments of 802.11b/g wireless protocols have pushed the evolution of multi-band antennas [9, 10]. In addition, dual band operation is a solid advantage for positioning technology, as testified in [11], where a dual band radio operating in 2.45 and 5.7 GHz is successfully employed in indoor scenarios to improve the Direction of Arrival estimation accuracy. Usually when applied to this class of positioning system a set of N antenna elements is typically arranged in a regular architecture, to form a Switched Beam Antenna (SBA), which is the key component for space division multiple access (SDMA) technology [7, 12]. Thanks to the regular arrangement, SDMA is easily implemented selectively enabling the signal reception from a specific antenna, thus isolating the signal coming from a specific angular region. At the same time the N beams must be large enough to cumulatively cover the entire 360° angle, permitting to operate without blind areas. This approach mitigates the uncertainty due to the multiple path reception [13], which is a perfect match for the cross-polarization rejection characteristics of CP antennas.

In view of these considerations, we propose a compact antenna with enhanced gain and circular polarization purity at 2.45 and 5.10 GHz, suitable for DualBand 802.11 WiFi operations. While many designs for dual band patches can be found in literature [14, 15], they typically suffer from the lack of an adequate number of parameters to successfully satisfy gain, polarization purity and matching requirements at the two operation frequencies. More effective solutions, such as the one proposed in [16], are based on a stacked structure, a solution which could potentially limit the antenna integration.

The proposed antenna is based on a design originally proposed by one of the authors, further enhanced with two additional features. The first enhancement is the strategy originally proposed in [14],

Received 1 March 2017, Accepted 12 April 2017, Scheduled 28 April 2017

^{*} Corresponding author: Stefano Maddio (stefano.maddio@unifi.it).

The authors are with the Department of Information Engineering, University of Florence, Via S. Marta Florence, Italy.

consisting in exploiting two pairs of narrow slits close to the radiating edges. Furthermore, in [17], a design based on the gap-coupling mechanism of parasitic patches was proposed. The additional patches, coupled by proximity, permit a fine-tuning of the second resonant frequency and an enhancement of the realized gain. To validate the proposed design, a single-layer via-less prototype is fabricated. Measurements show a realized gain of 6.15 dB and 5.9 dB respectively at 2.45 GHz and 5.10 GHz, with axial ratio below 0.5 dB as well as return losses of 15 dB.

2. BASIC DESIGN

The core of the design is the circular patch in Figure 1(a), consisting of a disc with an elliptic hole at its center. This kind of design was introduced in [17–19], hence it is only briefly summarized in this section. The disc radius is R , while the ellipse axes are A and B . The central hole operates as a modal degeneration driver, perturbing the fundamental mode, TM_{11} . In unperturbed conditions, the resonant frequencies of the modes of a disc patch are dictated by the dimension R as well as by the dielectric characteristic of the substrate [20].

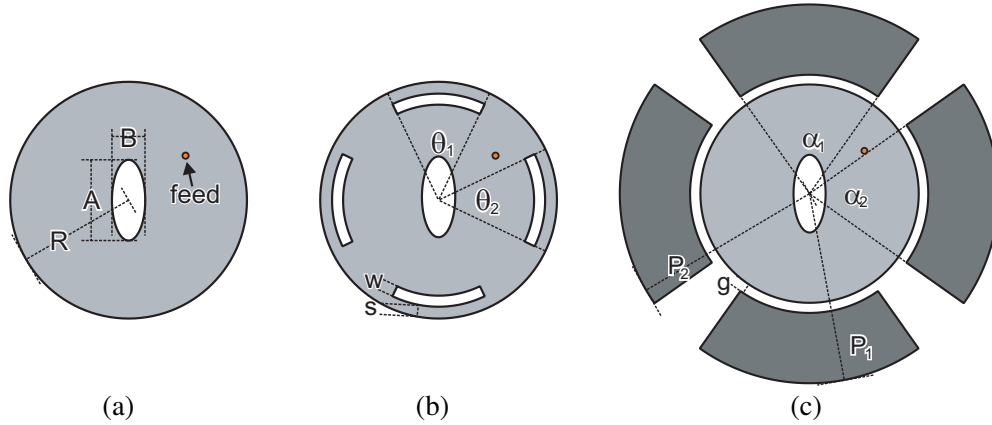


Figure 1. Patch design evolution. (a) Basic disc design with the elliptical cut. (b) Enhanced design with the arc-shaped slits. (c) Enhanced design with the gap-coupled parasitic patches.

Because of the quasi-symmetrical perturbation induced by the ellipse, the fundamental mode is divided in two orthogonal components, labeled as TM_{1x} and TM_{1y} . Their respective resonant frequencies f_1 and f_2 still depends on R , but are also inversely proportional to A and B [19]. When both modes are excited with the same magnitude and in phase quadrature, the resulting far-field is in a perfect CP condition [20].

Figure 2 shows the results of parametric analysis on the major axis A , when the disc radius and the other axis B are fixed. In particular the left-hand component of the broadside far-field is reported for a

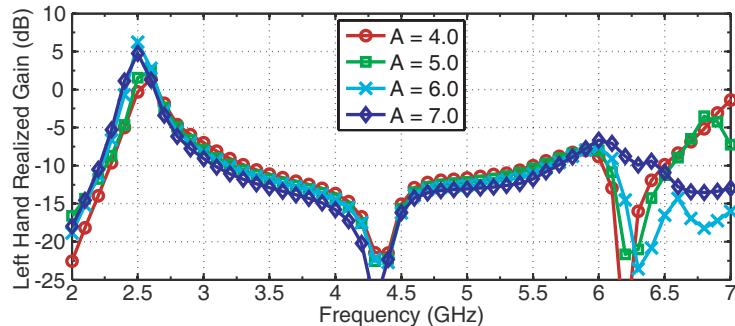


Figure 2. Broadside gain vs frequency for the basic design, Figure 1(a).

wide range of frequency. It can be observed that the modes TM_{1x} and TM_{1y} , excited around 2.5 GHz, are heavily affected by the ellipse dimension, resulting in a constructive far-field for $A = 4.5$ mm. However, inspecting Figure 2 it can be concluded that this design is not capable to independently control the TM_{11} and the TM_{12} , which is the second mode suitable for broadside radiation after the fundamental one. As expected for the canonical disc case, as the f_{12}/f_{11} ratio is actually dictated by the zeros of the Bessel functions [20]. Since this design is not capable to independently control the TM_{11} and TM_{12} modes, neither of the two pairs of degenerated modes can be successfully tuned.

3. ENHANCED DESIGN

Starting from the basic design, two kind of enhancements are applied to the disc patch, in order to control both the pairs of degenerated modes at the two different modal resonances.

3.1. Design with the Arc-Shaped Slits

An effective strategy to obtain dual-band operation is based on the use of arc-shaped slots, firstly proposed in [14], and then further developed in [15], for antennas operating in CP.

With reference to Figure 1(b), this design solution considers two pairs of narrow arc-shaped slots etched parallel to the four radiating edges of the disc patch. The first pair, placed near the “north” and “south” boundaries, is subtended by an angle θ_1 ; the second one, placed near the “east” and “west” boundaries is subtended by θ_2 . The slots have width w and distance s from the edge.

According to [15], the dual-frequency operation is associated with the different effect that the slits induce on the TM_{11} and on the TM_{12} mode. Since the slots are etched close to the radiating edges, where the TM_{11} modal currents are at their minimum, the characteristics of this mode are only slightly affected, and the radiative phenomena are almost the same as that of an unperturbed patch.

On the other hand, the modal currents of the TM_{12} mode, which are significant close to the edge, are strongly modified, since they are forced to circulate around the slots. This condition forces them to produce a null close to the edge of the slots, modifying the current distribution at the center of the patch. In particular, they assume a distribution similar to the one of the unperturbed TM_{11} mode, which can be controlled with the degree of freedom given by the slits angle θ for the tuning of resonance frequency [14].

Figure 3 shows the results of a parametric analysis, carried out with $\theta_1 = \theta_2$ for the sake of simplicity. Observing the broadside gain it can be noted how the arc angle parameter is effective in modifying the patch higher mode, while it has almost no effect on the first mode. This latter result is in agreement with the analysis proposed in [15], where the degeneration driver is not an ellipse but a small protuberance in the west slit. Exploiting all the degrees of freedom, letting also $\theta_1 \neq \theta_2$, it is possible to achieve a good performance at the desired frequencies. However, despite the capability of roughly satisfactory requirements at both frequencies, this architecture cannot effectively produce the best radiation characteristics in term of maximum gain and polarization purity.

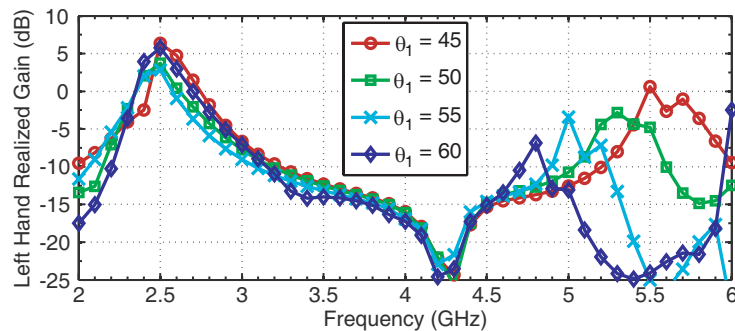


Figure 3. Broadside gain vs frequency for the design with the slits, Figure 1(c).

3.2. Design with the Parasites

With reference to Figure 1(c), four parasitic patches are arranged as two pairs of opposite circular sectors around the principal patch. Each pair of parasites is design to be coupled with a degenerated mode originated by the split of the fundamental one. Exploiting the additional area, the principal effect of the gap-coupled parasites is to enhance the radiation properties [21,22]. In particular, the antenna gain is increased without sacrificing too much area, exploiting the passive effect array. Gain improvements above 1 dB without incrementing the PCB area were demonstrated in [17]. This kind of design can be regarded as a passive array-like structure, in which the parasitic patches are excited by the gap-coupling mechanism.

Due to the nature of the gap-coupling mechanism, the sets of parasites perturb the TM_{12} degenerated modes in a different way with respect to the slits, and their effect is also sensible on the TM_{11} modes.

Considering the presence of the elliptical cut, which control the degeneration of the fundamental TM_{11} mode, but which affect also the TM_{12} mode, it is quite difficult to predict the behavior of the parasitic-loaded design. The results of the parametric analysis in Figure 4, carried out for $\alpha_1 = \alpha_2$, with α_1 varying from 40° to 70° , confirms the impact that the patches have on both the TM_{11} and TM_{21} mode. As expected for the passive-array model, the far-fields of the degenerated modes at the two frequencies are enhanced, thanks to the increase of active area. Unfortunately, it is difficult to control this effect for both the modal resonances.

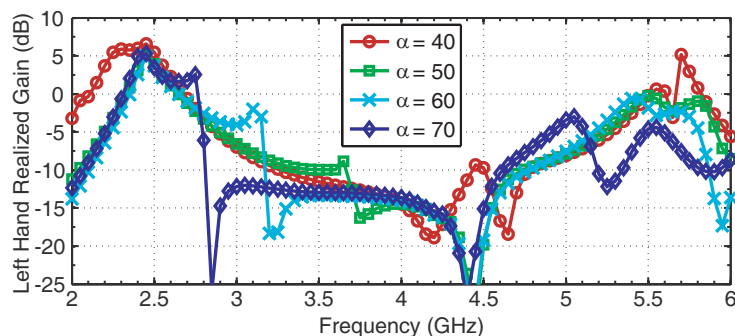


Figure 4. Broadside gain vs frequency for the design with the parasites, Figure 1(c).

3.3. Design with Arc-Shaped Slits and Parasites

To address the problem of the critical trade-off of the constraints at the two frequencies, the combination of slits and parasites is employed. Considering that the elliptical cut acts primarily on the first mode, (cfr. Section 2), while the slits operate primarily on the second one (cfr. Section 3.1), the combination of the two designs grant the flexibility required to control both of them. Furthermore, the parasitic mechanism can be tuned to affect both the resonant frequency, resulting in a more than adequate set of parameters.

With reference to Figure 5(a), the four parasitic patches are arranged to match the slits position on the four *edges* of the disc. Parasites and slits operate on both the TM_{11} and TM_{12} modal pairs, combining the beneficial of the increased area with the fine tuning mechanism of the slits.

The conditions to impose for the two resonances are not independent, but thanks to the large number of parameters, a satisfactory combination of resonances is possible, combining the beneficial effects of the two independent mechanisms described in the previous sections. With reference to Figure 6, four sets of θ and α are identified. The proposed set permits to impose the same frequency of 2.45 GHz for the first resonance and various frequency between 4.8 GHz and 5.3 GHz for the second resonance. The gain is about 4.5 dB for 2.45 GHz while exceeds 3 dB for the cases around 5.0 GHz.

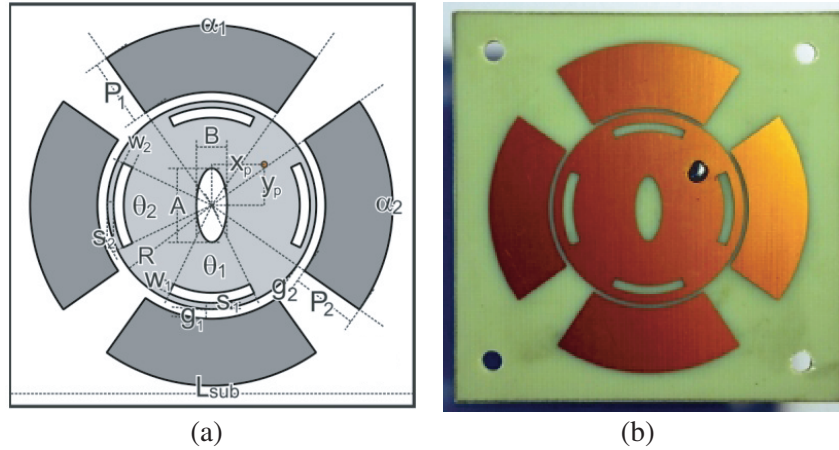


Figure 5. Proposed antenna design and realization. All dimensions in mm and degrees. (a) Layout with slits and parasites. (b) Photo of the prototype.

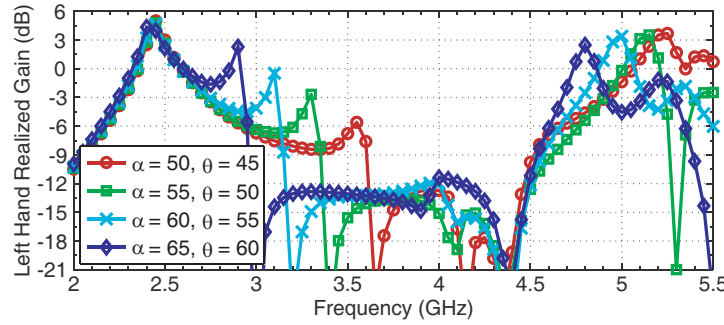


Figure 6. Broadside gain vs frequency for the design with slits and parasites.

4. EXPERIMENTAL VALIDATION OF THE FINAL DESIGN

According to the parametric analysis in the previous sections, a design combining the advantages of both the slits and the parasites is assembled. Given the large number of constraints at the two frequencies of operation, a dedicated multi-objective approach for optimization, operating on concurrent parameters, has been carried out, following the strategy introduced in [23, 24] and further refined in [25].

With reference to Figure 5(a), the best parameter set, reported in Table 1, is selected after a full-wave optimization. The corresponding prototype depicted in Figure 5(b) is fabricated using standard photo-etching technique on a commercial substrate ($\epsilon_r = 3.65$, $\tan \delta = 0.01$, height = 1.6 mm).

Table 1. List of the geometric parameters of the antenna design. All dimension in mm and degree.

R	A	B	x_p	y_p	w_1	w_2	s_1	s_2
16.17	11.04	4.55	7.78	6.08	1.51	1.82	1.63	1.61
θ_1	θ_2	g_1	g_2	α_1	α_2	P_1	P_2	L_{sub}
51.3	51.6	0.72	0.73	67.4	70.5	10.93	9.98	65

The measured patterns at the frequencies of 2.45 GHz and 5.10 GHz are shown in Figure 7(a) and Figure 7(b), respectively. Both the co-polar left hand and cross-polar right-hand components are shown, demonstrating the good cross-polarization discrimination (XPD) in the boresight direction.

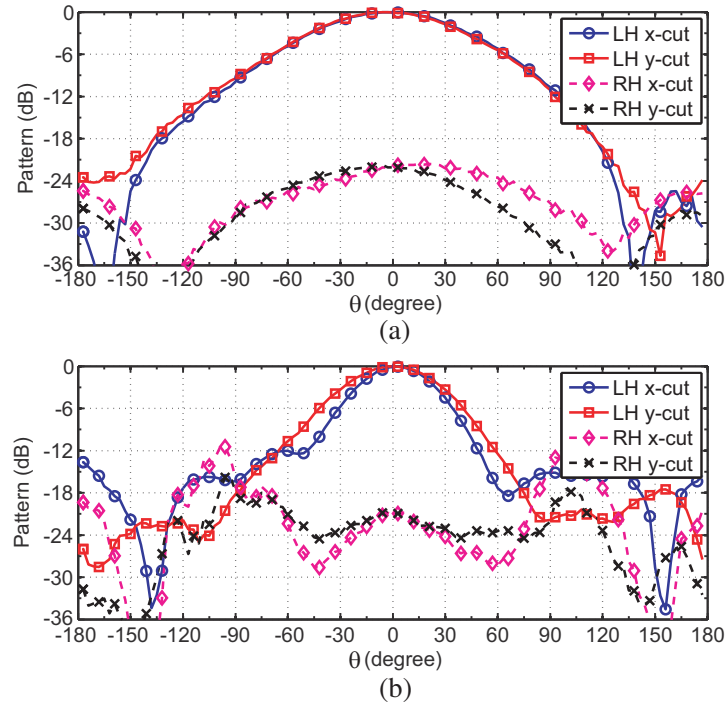


Figure 7. Realized gain of the proposed dual-band antenna. (a) Radiation pattern at 2.45 GHz. (b) Radiation pattern at 5.10 GHz.

The different behaviors of the TM_{11} and TM_{12} modes is clearly visible. In particular, when operating at 2.45 GHz, the XPD is 22 dB in boresight, and about 19 dB within the Half Power Beam Width. Furthermore, the XPD is in excess of 15 dB, meaning an axial ratio below 3 dB, within the range -90° to 90° . Focusing on the operation at 5.1 GHz, the XPD exceeds 21 dB in boresight direction, and it is equal to 15 dB within the range between -45° and 45° , corresponding to the most of the main lobe.

The measured gain in the bore-sight direction versus frequency is depicted in Figure 8, along with the axial ratio. The realized result is in very good matching with the simulations, keeping also the same sharp second maximum in the first operation bandwidth.

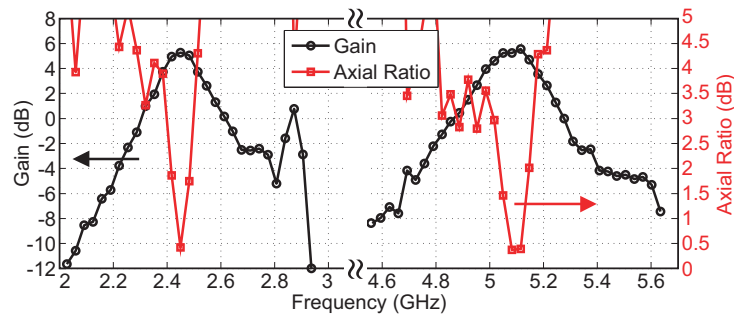


Figure 8. Broadside gain and axial ratio vs frequency for the realized prototype.

The good polarization performance is confirmed, as well as an adequate bandwidth, compatible with the modal degeneration operation. The return loss, not shown for space reasons, is about 15 dB at both 2.45 GHz and 5.10 GHz with a 10 dB bandwidth of 100 MHz and 170 MHz, respectively.

5. CONCLUSIONS

A circular polarized patch antenna suitable for dual-band operation is proposed in this paper. The circular polarization is driven by the modal degeneration operating on the TM_{11} and TM_{12} modes. The design of the antenna is based on the combination of the arc-slitted approach and gap-coupled strategy. The experimental validation confirms a good performance: the radiation patterns are symmetric, with a maximum realized gain of 5.9 dB at 2.45 GHz and 6.15 dB at 5.10 GHz. In both cases 0.5 dB of axial ratio and 15 dB of return loss are measured at the center frequencies.

REFERENCES

1. Chizhik, D., J. Ling, and R. A. Valenzuela, "The effect of electric field polarization on indoor propagation," *Proc. IEEE Int. Conf. on Universal Personal Communications*, 459–462, Florence, Italy, October 1998.
2. Gaspard, I., "Polarization properties of the indoor radio channel," *2015 IEEE International Conference on Microwaves, Communications, Antennas and Electronic Systems (COMCAS)*, 1–5, IEEE, 2015.
3. Zhong, Z. and X. Liao, "Circular polarization benefits in outdoor to indoor scenarios for MIMO cellular networks," *2014 Sixth International Conference on Wireless Communications and Signal Processing (WCSP)*, 1–5, IEEE, 2014.
4. Rappaport, T. and D. Hawbaker, "Wide-band microwave propagation parameters using circular and linear polarized antennas for indoor wireless channels," *IEEE Transactions on Communications*, Vol. 40, No. 2, 240–245, 1992.
5. Blanco, M., R. Kokku, K. Ramachandran, S. Rangarajan, and K. Sundaresan, "On the effectiveness of switched beam antennas in indoor environments," *Springer Proc. International Conference on Passive and Active Network Measurement*, Vol. 57, No. 5, 122–131, 2008.
6. Gotsis, K. A., K. Siakavara, and J. N. Sahalos, "On the direction of arrival (DoA) estimation for a switched-beam antenna system using neural networks," *IEEE Transactions on Antennas and Propagation*, Vol. 57, No. 5, 1399–1411, 2009.
7. Maddio, S., M. Passafiume, A. Cidronali, and G. Manes, "A scalable distributed positioning system augmenting WiFi technology," *2013 International Conference on Indoor Positioning and Indoor Navigation (IPIN)*, 1–10, IEEE, 2013.
8. Heidari, A. A., M. Heyrani, A. Cidronali, and M. Nakhkash, "A dual-band circularly polarized stub loaded microstrip patch antenna for GPS applications," *Progress In Electromagnetics Research Letters*, Vol. 92, 195–208, 2009.
9. Ren, W., "Compact dual-band slot antenna for 2.4/5 GHz WLAN applications," *Progress In Electromagnetics Research B*, Vol. 8, 319–327, 2008.
10. Zhao, G., F. S. Zhang, Y. Song, Z. B. Weng, and Y. C. Jiao, "Compact ring monopole antenna with double meander lines for 2.4/5 GHz dual-band operation," *Progress In Electromagnetics Research*, Vol. 72, 187–194, 2007.
11. Cidronali, A., G. Collodi, S. Maddio, M. Passafiume, G. Pelosi, and S. Selli, "Improving phaseless DoA estimation in multipath-impaired scenarios by exploiting dual-band operations," *2016 IEEE MTT-S International Microwave Symposium (IMS)*, 1–4, 2016.
12. Brs, L., N. B. Carvalho, P. Pinho, L. Kulas, and K. Nyka, "A review of antennas for indoor positioning systems," *International Journal of Antennas and Propagation*, Vol. 2012, 2012.
13. Maddio, S., A. Cidronali, and G. Manes, "Smart antennas for direction of arrival indoor positioning applications," *Handbook of Position Location: Theory, Practice, and Advances*, 319–355, 2011.
14. Maci, S., G. B. Gentili, P. Piazzesi, and C. Salvador, "Dual-band slot-loaded patch antenna," *IEE Proceedings — Microwaves, Antennas and Propagation*, Vol. 142, No. 3, 225–232, 1995.
15. Hsieh, G.-B., M.-H. Chen, and K.-L. Wong, "Single-feed dual-band circularly polarised microstrip antenna," *IET Electronics Letters*, Vol. 34, No. 12, 1170–1171, 1998.

16. Pozar, D. M. and S. M. Duffy, "A dual-band circularly polarized aperture-coupled stacked microstrip antenna for global positioning satellite," *IEEE Transactions on Antennas and Propagation*, Vol. 45, No. 11, 1618–1625, 1997.
17. Maddio, S., "A compact circularly polarized antenna for 5.8 GHz intelligent transportation system," *IEEE Antennas and Wireless Propagation Letters*, Vol. 16, 533–536, 2017.
18. Maddio, S., A. Cidronali, and G. Manes, "A new design method for single-feed circular polarization microstrip antenna with an arbitrary impedance matching condition," *IEEE Transactions on Antennas and Propagation*, Vol. 59, No. 2, 379–389, 2011.
19. Maddio, S., "A circularly polarized antenna array with a convenient bandwidth/size ratio based on non-identical disc elements," *Progress In Electromagnetics Research Letters*, Vol. 57, 47–54, 2015.
20. Garg, R., *Microstrip Antenna Design Handbook*, Artech House, 2001.
21. Kumar, G. and K. C. Gupta, "Broad-band microstrip antennas using additional resonators gap-coupled to the radiating edges," *IEEE Transactions on Antennas and Propagation*, Vol. 32, No. 12, 1375–1379, 1984.
22. Maddio, S., "A circularly polarized switched beam antenna with pattern diversity for WiFi applications," *IEEE Antennas and Wireless Propagation Letters*, Vol. 16, 125–128, 2017.
23. Matekovits, L., M. Mussetta, P. Pirinoli, S. Selleri, and R. Zich, "Improved PSO algorithms for electromagnetic optimization," *2005 IEEE Antennas and Propagation Society International Symposium*, Vol. 2, 33–36, 2005.
24. Selleri, S., M. Mussetta, P. Pirinoli, R. E. Zich, and L. Matekovits, "Differentiated meta-PSO methods for array optimization," *IEEE Transactions on Antennas and Propagation*, Vol. 56, No. 1, 67–75, 2008.
25. Agastra, E., G. Pelosi, R. Taddei, and S. Selleri, "Taguchi's method for multi-objective optimization problems," *International Journal of RF and Microwave Computer-aided Engineering*, Vol. 23, No. 3, 357–366, May 2013.